Role of Halogen Bonds in Thyroid Hormone Receptor Selectivity: Pharmacophore-Based 3D-QSSR Studies

Napoleão F. Valadares,* Lívia B. Salum, Igor Polikarpov, Adriano D. Andricopulo, and Richard C. Garratt

Centro de Biotecnologia Molecular Estrutural, Departamento de Física e Informática, Instituto de Física de São Carlos, Universidade de São Paulo, Av. Trabalhador São-Carlense 400, 13560-970 São Carlos-SP, Brazil

Received August 21, 2009

Most physiological effects of thyroid hormones are mediated by the two thyroid hormone receptor subtypes, TRα and TRβ. Several pharmacological effects mediated by TRβ might be beneficial in important medical conditions such as obesity, hypercholesterolemia and diabetes, and selective TRβ activation may elicit these effects while maintaining an acceptable safety profile. To understand the molecular determinants of affinity and subtype selectivity of TR ligands, we have successfully employed a ligand- and structure-guided pharmacophore-based approach to obtain the molecular alignment of a large series of thyromimetics. Statistically reliable three-dimensional quantitative structure−activity relationship (3D-QSAR) and three-dimensional quantitative structure-selectivity relationship (3D-QSSR) models were obtained using the comparative molecular field analysis (CoMFA) method, and the visual analyses of the contour maps drew attention to a number of possible opportunities for the development of analogs with improved affinity and selectivity. Furthermore, the 3D-QSSR analysis allowed the identification of a novel and previously unmentioned halogen bond, bringing new insights to the mechanism of activity and selectivity of thyromimetics.

INTRODUCTION

As part of the nuclear receptor superfamily, the thyroid hormone receptors (TRs) are ligand-modulated transcriptional regulators involved in cell differentiation, development, metabolism, and the physiological function of most tissues.[1,2] To mediate activation or repression of specific target genes, these receptors associate with several transcriptional coregulatory complexes in a hormone dependent way. Although nongenomic actions of the thyroid hormones can also modulate important signaling pathways,[3] most of their physiological effects are mediated by the two TR subtypes, TRα and TRβ.[2,4]

Many lines of evidence demonstrate that several pharmacological actions of TRs might be beneficial in medical therapy, particularly those mediated by TRβ that are related to important conditions like obesity, hypercholesterolemia and diabetes.[4−8] Additionally, the findings that TRα is the predominant isoform in the heart and mediates most of the deleterious cardiovascular effects of thyroid hormones[2,9] have strongly stimulated the search for selective TRβ ligands, which could address important medical needs with an acceptable safety profile.[8] Indeed, recent studies presented the synthesis of structurally related TRβ selective ligands based on structure−activity relationships and structural studies.[10−14] Significantly, Sobetirome (GC-1), one of the most studied selective thyromimetics, completed phase 1 clinical trials in 2008 and is currently being considered as a novel potent cholesterol lowering agent.[5,15,16]

X-ray structures of the ligand binding domain of the TRs in complex with agonists show the ligand completely enclosed within a lipophilic binding pocket in the ligand binding domain (LBD) and that these receptors present enough flexibility to accommodate different ligands.[10,17,18] In fact, upon agonist binding the receptor undergoes extensive structural changes, repositioning Helix 12 (H12) over the lower part of helices 3 and 5, where it participates in the formation of the surface for coactivator recognition and binding (AF-2).[19] Thus, TR flexibility plays an important role in ligand binding and dissociation, and the ligand induced conformational changes are fundamental for receptor interaction with coregulators.[18,20−23]

Quantitative structure−activity relationship (QSAR) methods have been widely used as valuable tools to assist the design of receptor ligands with improved properties and potential utility in clinical medicine.[24−26] Comparative molecular field analysis (CoMFA)[27,28] is one of the most popular three-dimensional quantitative structure−activity relationship (3D-QSAR) methods, having a number of promising attributes, including the possibility of visualizing the regions in space responsible for increases or decreases in the values of a particular biological property. Although we have presented predictive 2D-QSAR models for both TRα and TRβ,[29] the development of 3D-QSAR models with internal and external consistency for both isoforms proved to be a major challenge, mainly because the 3D methods are dependent on how the ligand conformations are aligned with respect to one another in Cartesian space. The considerable conformational adjustments in the receptors necessary to accommodate different ligands, which involve changes to both amino acid side chain conformations[11,30] and the

* To whom correspondence should be addressed. E-mail: napoleao@mac.com. Phone: + 55 16 3373. Fax: + 55 16 3373-9881.

10.1021/ci900316e CCC: $40.75
Published on Web 10/28/2009

relative positions of helices,[17] add further complexity to the use of conventional structure-based approaches to generate the 3D molecular alignment.

In the present work, we describe a ligand- and structure-guided pharmacophore-based approach to address these difficulties, which made it possible to successfully employ the CoMFA method to obtain statistically reliable models for both TR isoforms. Most importantly, the methodology described here allowed us to derive a consistent three-dimensional quantitative structure-selectivity relationship (3D-QSSR) model for a large series of thyromimetics, and the graphical analysis of these models highlighted a number of possibilities for developing analogs with improved affinity and selectivity.

RESULTS AND DISCUSSION

Data Set Characterization. 3D QSAR and QSSR CoMFA models were derived for a series of 69 thyroid receptor modulators for which binding affinity for both TRα and TRβ were determined under the same experimental setup[10−14] (Table 1). The IC_{50} values are adequately distributed across a particularly wide potency range, varying from 0.031 nM to 160 μM for TRα (∼8 orders of magnitude) and from 0.019 nM to 32 μM for TRβ (∼7 orders of magnitude). The TRβ selectivity values vary from 0.54 to 38. The 69 thyroid receptor ligands were divided into a training set for model construction containing 55 compounds (**1**−**55**, Table 1) and a test set for external model validation containing the remaining 14 compounds (**56**−**69**, Table 1). Hierarchical cluster analyses performed with TSAR 3D (Accelrys, San Diego, USA) were used as previously described to guide appropriate compound selection for developing all QSAR and QSSR models.[26] These analyses guarantee that both training and test sets represent the structural diversity and cover the whole data set potency and selectivity space, rendering the data set appropriate for the purpose of QSAR model development, as depicted in Figure 1. It is important to note that the same training and test sets were employed for all 3D QSAR analyses. The IC_{50} values were converted into the corresponding pIC_{50} ($-\log IC_{50}$) values and the selectivity values were converted into logarithm of the selectivity (log *S*) values prior to their use as dependent variables in the investigations.

Pharmacophore Model. One of the most significant drawbacks of the CoMFA method is its sensitivity to the alignment of the molecules in the data set. The very necessity of having an aligned data set is a significant limitation, as some data sets might not be readily aligned. In the case of the present data set, neither rigid-body fitting[31] nor structure-based alignment strategies[32] provided predictive models because of the significant structural diversity of the compounds, the considerable size of some analogs and due to the conformational adjustments in the receptors necessary to accommodate different ligands. These approaches generated unrealistic and visually incorrect alignments, and the 3D QSAR models obtained using these alignments presented poor external validation. A pharmacophore-based strategy was then employed in an attempt to circumvent the disadvantages of the automated alignment and structure-based methods for this specific data set of thyromimetics.

The information provided by a crystal complex of a bioactive compound bound to its target protein can be used to define the chemical landscape of the binding cavity and consequently to determine complementary characteristics required in small molecule modulators.[33] Currently, crystal complexes for two compounds in the data set with both human TRα and TRβ are known (PDB codes 1NAV, 1NAX, 2H79, 1XZX).[10,30,34] In these complexes, compound **1** (3,5,3′-Triiodo-L-thyronine, the most active of the thyroid hormones, also known as T3) and compound **7** (also known as KB-141), one of the most studied TRβ selective thyromimetic,[5−7] interact with both TR isoforms in very similar conformations (compound **1** rmsd = 0.14 Å, compound **7** rmsd = 0.11 Å, Supporting Information Figure 1). The structure of compound **4** cocrystallized with TRβ (PDB code 2J4A)[35] also displays a striking resemblance to the crystal structures of compounds **1** and **7**. Furthermore, even for the crystal structure of TRβ in complex with compound **30**, in which the receptor presents significant conformational changes in order to accommodate this larger ligand,[11] the binding mode is very similar to that displayed by compounds **1** and **7** in complex with TRα or TRβ. This evidence, along with the observation that the internal hydrophobic ligand binding pockets of the TR isoforms are identical except for one residue (Ser277 in TRα is substituted by Asn331 in TRβ), encouraged us to select of a common pharmacophore hypothesis for both receptors.

The crystallographic structures[10,11,17,19,30,34−37] show the 4′-hydroxyl group of the ligand hydrogen bonding to a key histidine residue (His381 in TRα or His435 in TRβ), and its carboxylate group participating in a hydrogen bonding network which may involve arginine residues, water molecules and the β-hairpin presenting the only amino acid difference between both isoforms (Figure 2). The 3′ group occupies a region of the receptor that is flexible enough to accommodate substituents of different sizes, as illustrated by the compounds in the data set and crystallographic studies.[11,17]

Integration of ligand and structure-based information is a useful strategy in obtaining a pharmacophore model and a reliable molecular alignment. Considering a data set with broad structural diversity and a very flexible target receptor, the selection of several features based on a special group of molecules or specific receptor conformation tends to be excessively restrictive to fit diverse molecules. In the present study, superposition of different subsets of structurally representative ligands was carried out based on shared pharmacophore features using the GALAHAD program. The final pharmacophore hypothesis constructed with the program UNITY is depicted in Figure 3, and was employed in the development of the CoMFA models.

The final pharmacophore hypothesis represents the 4′ hydroxyl and the 3′ steric group in the distal ring, the acidic function that participates in a number of strong polar interactions and the three-dimensional disposition of the diphenyl ether moiety, described by both aromatic rings present in most molecules in the data set as well as the ether oxygen linking these rings. In order to correctly describe the smallest compounds in the data set, fulfilling the features on the distal ring was made optional.

CoMFA Models. The molecular alignment depicted in Figure 4 for the 55 training set thyromimetics was employed in several PLS analyses carried out using the CoMFA method. The models were optimized using the CoMFA

Table 1. Chemical Structures and Corresponding pIC_{50} and log *S* Values of the TRα and TR*β* Ligands Used for 3D-QSAR Studies[a]

Training Set Compounds

Cpd	Structure	pIC_{50} TRα	pIC_{50} TRβ	log*S*	Cpd	Structure	pIC_{50} TRα	pIC_{50} TRβ	log*S*
1	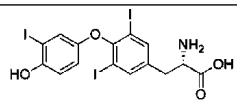	9.62	9.58	-0.27	**2**	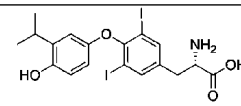	9.85	9.96	-0.12
3	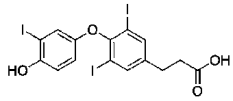	10.39	10.72	0.1	**4**	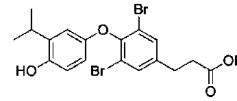	10	10.6	0.37
5	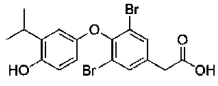	8.85	10.02	0.94	**6**	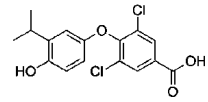	6.89	7.68	0.56
7	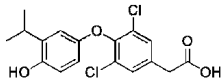	7.6	8.96	1.13	**8**	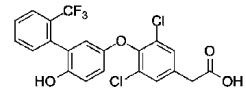	7.74	8.49	0.52
9	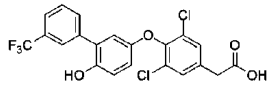	7.4	9.07	1.44	**10**	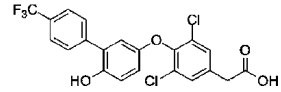	6.29	7.17	0.65
11	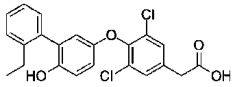	7.89	9.7	1.58	**12**	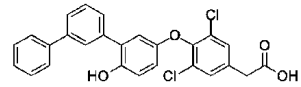	6.34	7.68	1.11
13	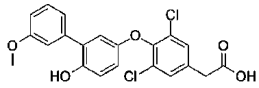	6.53	7.96	1.2	**14**	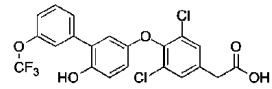	7	8.47	1.24
15	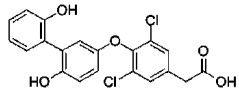	5.98	7.3	1.09	**16**	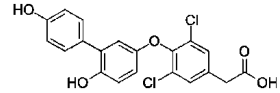	6.07	7.06	0.76
17	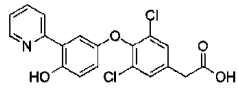	5.82	6.86	0.81	**18**	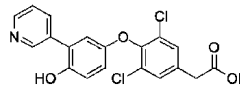	6.09	7.39	1.07
19	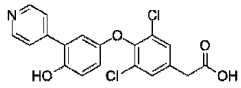	6.84	6.91	-0.16	**20**	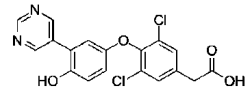	6.57	7.17	0.37
21	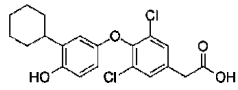	6.59	8.11	1.29	**22**	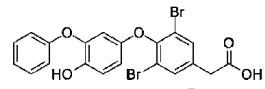	6.91	8.22	1.08
23	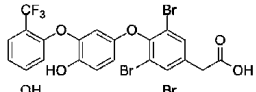	6.61	8.12	1.28	**24**	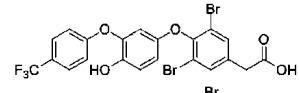	6.47	8.02	1.32
25	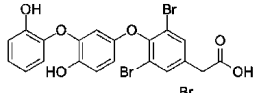	5.83	7.08	1.02	**26**	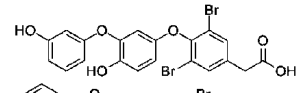	6.26	7.33	0.84
27	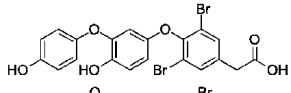	6.62	8.22	1.37	**28**	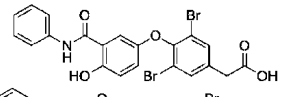	6.37	7.45	0.85
29	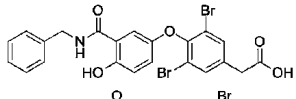	7.07	8.38	1.08	**30**	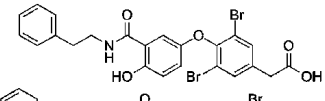	7.82	9.21	1.16
31	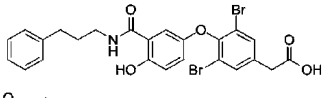	6.69	8.17	1.25	**32**	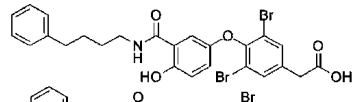	6.55	7.74	0.96
33	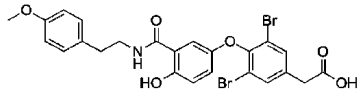	6.64	7.43	0.56	**34**	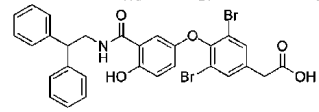	7.74	9.33	1.36
35	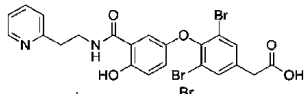	5.94	7.17	1	**36**	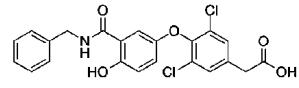	6.9	8.46	1.33
37	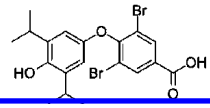	5.8	6.04	0.01	**38**	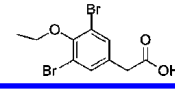	3.8	4.49	0.46

Table 1. Continued

Cpd	Structure	pIC_{50} TRα	pIC_{50} TRβ	log*S*	Cpd	Structure	pIC_{50} TRα	pIC_{50} TRβ	log*S*
Training Set Compounds									
39	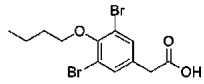	4.58	5.72	0.91	**40**	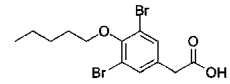	4.7	5.24	0.31
41	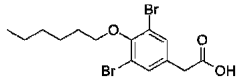	5.28	5.82	0.31	**42**	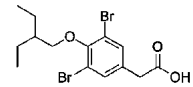	5.16	6.1	0.71
43	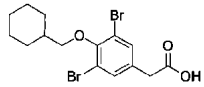	5.57	6.11	0.31	**44**	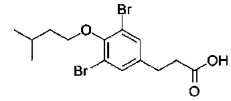	5.36	5.74	0.15
45	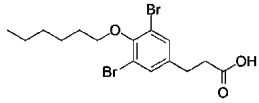	5.96	6.44	0.25	**46**	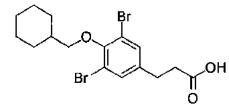	6.34	6.72	0.15
47	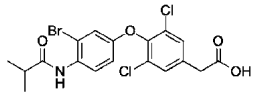	6.2	7.74	1.31	**48**	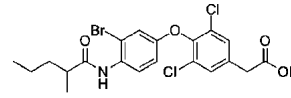	6.62	8.37	1.52
49	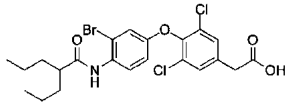	5.92	7.35	1.2	**50**	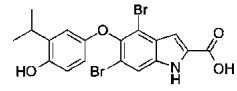	8.6	9.55	0.72
51	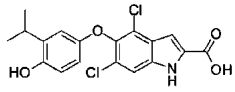	8.85	10.22	1.14	**52**	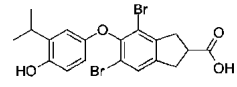	7.42	8.07	0.42
53	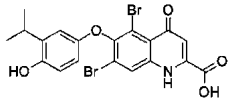	6.6	7.29	0.46	**54**	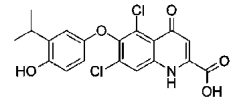	5.46	6.06	0.37
55	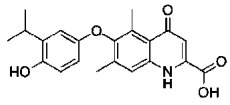	6.21	6.62	0.18					
Test Set Compounds									
56	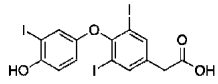	9.85	10.39	0.31	**57**	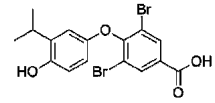	8.01	8.68	0.44
58	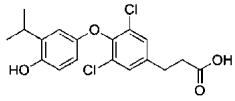	9.12	9.82	0.47	**59**	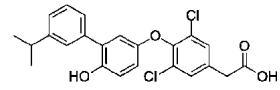	6.91	8.4	1.26
60	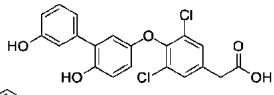	5.93	7.12	0.96	**61**	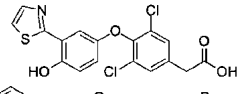	6.25	7.55	1.07
62	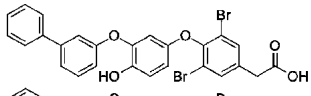	6.3	7.22	0.69	**63**	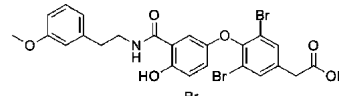	7.03	8.31	1.05
64	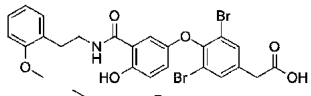	7.02	8.07	0.82	**65**	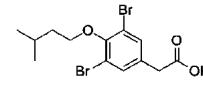	4.89	5.74	0.62
66	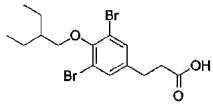	5.8	6.09	0.06	**67**	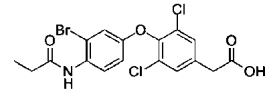	5.48	6.85	1.14
68	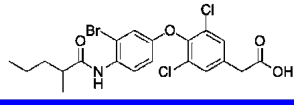	5.89	7.33	1.21	**69**	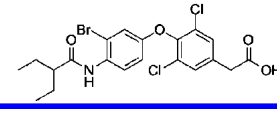	6.21	7.8	1.36

[a] Cpd = compound; $pIC_{50} = -\log(IC_{50})$; selectivity is defined[10] as $IC_{50}(TR\alpha)/(IC_{50}(TR\beta) \times 1.7)$; log *S* = logarithm of the selectivity.

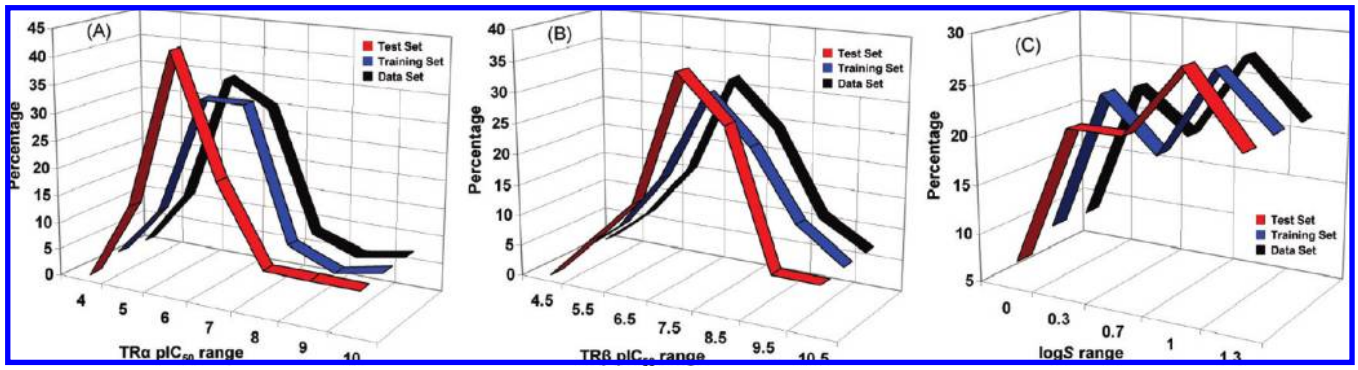

Figure 1. Distribution of the biological property values for the training set (blue), test set (red), and complete data set (black). (A) pIC_{50} TRα, (B) pIC_{50} TRβ, and (C) log *S*.

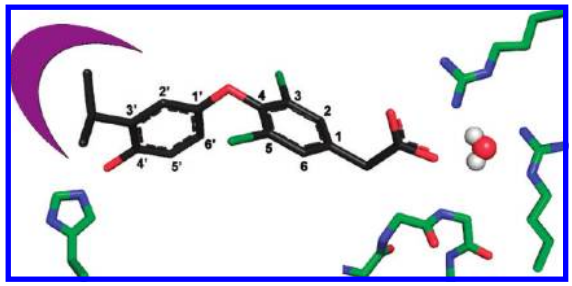

Figure 2. Simplified scheme of the interactions of the data set ligands within the binding pocket of the TRα and TRβ. The affinities of the thyromimetics in the data set to the TRs is modulated by a number of factors, including the interaction of the 4′ hydroxyl group with a histidine residue, the nature of the substituent in the 3′ position and the hydrogen bonding network pattern induced by the group in the 1 position which may involve arginine residues, water molecules and residues from the β-hairpin. Compound **7** (KB-141) is ring numbered and shown as reference. The purple area represents the 3′ lipophilic binding pocket.

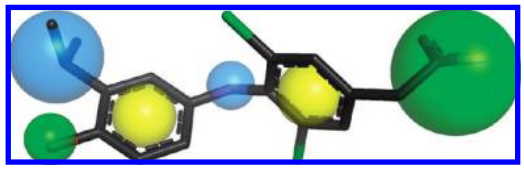

Figure 3. Compound **7** (KB-141) fitted by UNITY into the final pharmacophore hypothesis. The model contains 2 acceptors (green), 2 aromatic rings (yellow) and 2 steric surfaces (blue).

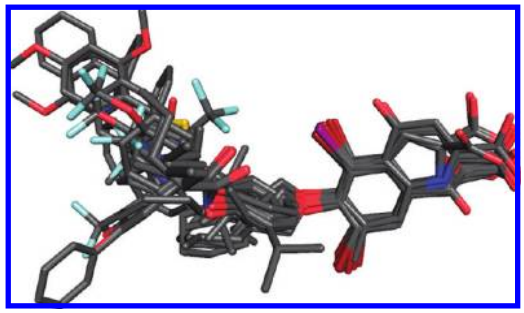

Figure 4. Molecular alignment generated by mapping the chemical features of the compounds to the pharmacophore model in UNITY.

region focusing method, which was weighted by StDev*Coefficient values ranging from 0.3 to 1.5, and grid spacings ranging from 0.5 to 2.0. This strategy not only increased q^2 values during the process of model generation, but also resulted in the refinement of 3D contour maps. The best statistical results are presented in Table 2. Statistically robust 3D QSAR and QSSR models were obtained using the

Table 2. CoMFA Results[a]

model	q^2	*N*	r^2	SEE	$r_{pred}{}^2$	fraction *S*	fraction *E*
(A) TRα	0.68	6	0.91	0.43	0.84	0.72	0.28
(B) TRβ	0.61	6	0.90	0.46	0.77	0.72	0.28
(C) selectivity	0.64	4	0.81	0.22	0.78	0.72	0.28

[a] q^2, Leave-one-out (LOO) cross-validated correlation coefficient; *N*, optimum number of components; r^2, non-cross-validated correlation coefficient; SEE, standard error of estimate; $r_{pred}{}^2$, predictive r^2; S, steric field; E, electrostatic field.

binding affinities for TRα and TRβ and the values of selectivity. As can be seen in Table 2, significant correlation coefficients were obtained, with a q^2 of 0.68 and an r^2 of 0.91 for the TRα model, as well as a q^2 of 0.61 and an r^2 of 0.90 for the TRβ model. Additionally, a q^2 of 0.64 and an r^2 of 0.81 were obtained for the selectivity model. The progressive scrambling method, applied to check for the possibility of correlations and to test the stability of the models, further confirmed their consistency as defined by the critical slope and the optimum statistics for cSDEP and Q**[2] obtained at the end of different runs. LMO procedures were performed as a more rigorous test of the stability and statistical significance of the model. The data set was divided into 10 (LMO_{10}) and 5 (LMO_5) randomly selected groups, and subsequently, each group was left out during the cross-validation process. Each model was evaluated 10 times by measuring its accuracy in predicting the activity of the remaining 10% or 20% of the training set. The results confirmed the stability of the 3D QSAR and QSSR models, since the statistical values obtained for the LMO analyses were comparable to those of the LOO analyses.

The predictive ability of the internally consistent CoMFA models generated employing the 55 training set molecules (compounds **1**−**55**, Table 1) was assessed by predicting the biological activities of an external test set (compounds **56**−**69**, Table 1), which was completely excluded during the generation of the models. Prior to prediction, the test set compounds were minimized with respect to their energy, aligned according to the constructed pharmacophore model and the partial charges were calculated identically to those of the training set. The results of the external validation process are listed in Table 3, and the graphic results simultaneously displayed in Figure 5. For the QSAR models, the predicted values fall close to the experimental pIC_{50} values, not deviating by more than one logarithm unit, except for compound **57**, for which the predicted value is more

Table 3. Experimental and Predicted Binding Affinities for TRα (αpIC_{50}) and TRβ (βpIC_{50}) and Selectivity Values (log *S*), with Residual Values for the Test Set Compounds

test set compound	αpIC_{50} exp[a]	αpIC_{50} predicted	residual[b]	βpIC_{50} exp[a]	βpIC_{50} predicted	residual[b]	log *S* exp[a]	log *S* predicted	residual[b]
56	9.85	8.94	0.91	10.39	9.41	0.98	0.31	0.50	−0.19
57	8.01	6.75	1.26	8.68	7.43	1.25	0.44	0.39	0.05
58	9.12	9.83	−0.71	9.82	10.68	−0.86	0.47	0.50	−0.03
59	6.91	7.18	−0.27	8.40	8.82	−0.42	1.26	1.29	−0.03
60	5.93	6.22	−0.29	7.12	7.25	−0.13	0.96	0.95	0.01
61	6.25	6.79	−0.54	7.55	7.98	−0.43	1.07	0.87	0.20
62	6.30	6.55	−0.25	7.22	7.86	−0.64	0.69	1.17	−0.48
63	7.03	7.04	−0.01	8.31	8.21	0.11	1.05	1.04	0.01
64	7.02	7.05	−0.03	8.07	8.34	−0.27	0.82	1.09	−0.27
65	4.89	4.37	0.52	5.74	5.33	0.41	0.62	0.57	0.05
66	5.80	5.86	−0.06	6.09	6.11	−0.02	0.06	−0.01	0.07
67	5.48	5.74	−0.26	6.85	7.41	−0.56	1.14	1.08	0.06
68	5.89	6.01	−0.12	7.33	7.84	−0.51	1.21	1.45	−0.24
69	6.21	5.86	0.35	7.80	7.76	0.04	1.36	1.46	−0.10

[a] Experimental data. [b] The difference between experimental and predicted values.

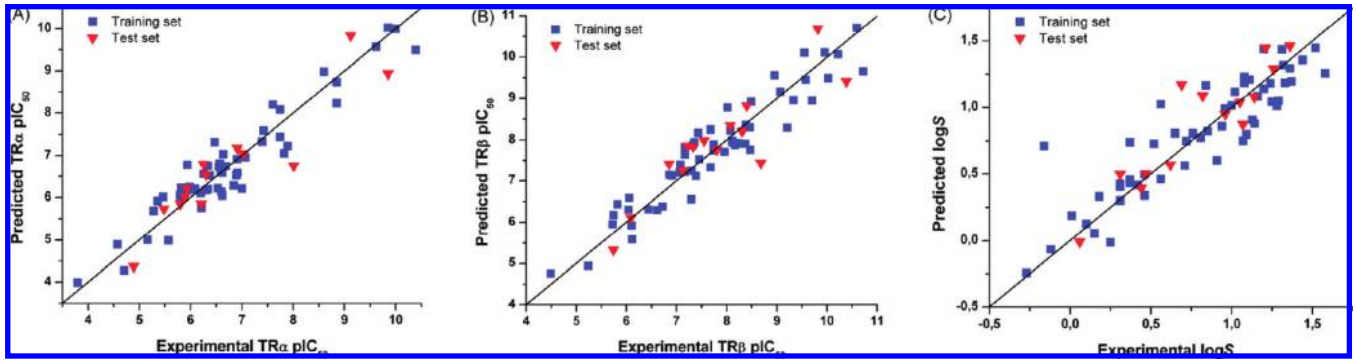

Figure 5. Plot of predicted values of pIC_{50} and log*S* versus the corresponding experimental values for the 55 training set compounds (blue squares) and the 14 test set compounds (red triangles). (A) TRα, (B) TRβ, and (C) selectivity.

substantially in error in both QSAR models. Predictive r^2 values of 0.84 and 0.77 were obtained for the TRα and TRβ CoMFA models, respectively. For the QSSR model, all residual values are lower than 0.5 log units, with an r_{pred}^2 of 0.78. The good agreement between actual and predicted pIC_{50} and selectivity values for the test set compounds in both the 3D QSAR and QSSR models suggests that the constructed models are reliable and can be used for the design of modulators with improved binding affinity and selectivity.

A CoMFA model for TRβ using a molecular alignment obtained by the rigid fit of a common substructure was previously reported.[38] It is important to mention that this data set is similar to the one used in our study,[10,11,13,14] except that all smaller compounds,[12] which do not present the selected common substructure, were removed. This exclusion not only reduced the structural diversity of the data set but also dramatically reduced the affinity interval more than 35 times. Even using a data set with higher structural diversity and affinity range, the pharmacophore derived method yielded a similar q^2 value and a significantly higher r_{pred}^2 value (0.77 versus 0.69), indicating a better external predictive power.

These results demonstrate the usefulness of the pharmacophore-based approaches to align structurally diverse and flexible compounds that present the same three-dimensional features, particularly if compared with the commonly employed rigid fit methods. With the use of available crystallographic information, the method is capable of representing the receptor−ligand interactions and aligning the data set molecules that present different chemical groups with the same pharmacophore characteristics.

3D Contour Maps. Besides their potential capability to predict the activities of untested molecules, the CoMFA models also shed some light on structural and chemical features that are directly related to biological activity, providing information about regions in space responsible for increases or decreases in the studied biological property. The contour maps presented here are displayed as PLS standard deviation × coefficient.

CoMFA Affinity Contour Maps. The CoMFA steric and electrostatic contour maps for both TRα and TRβ are shown in the Figure 6. The similarities between the steric and electrostatic contour maps for both isoforms are evident, which is a direct consequence of the high degree of similarity between the TRα and TRβ binding cavities and reflects the fact that the affinity determinants for these receptors share many common features. The regions where electropositive groups are favored and the regions unfavorable for steric interactions are located in the same position for both TR isoforms. Notice that the steric contour maps show a specific region near the 3′ position where bulky groups are allowed which is delimited by two unfavorable nearby areas (see also Supporting Information Figure 2). Moreover both contour maps present a region favorable for electronegative groups near the 4′ position where most data set analogs present a hydroxyl group. This expected feature shows that the QSAR modeling was able to identify and highlight the importance of a position occupied by an electronegative group in all

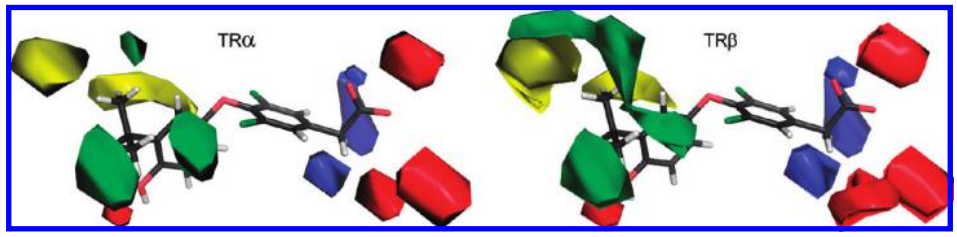

Figure 6. CoMFA contour maps for TRα (left) and TRβ (right). CoMFA steric contour maps are shown in yellow and green (contour levels −0.08 and 0.1, respectively) and CoMFA electrostatic contour maps are shown in red and blue (contour levels −0.05 and 0.05, respectively). Compound **7** (KB-141) is shown as reference.

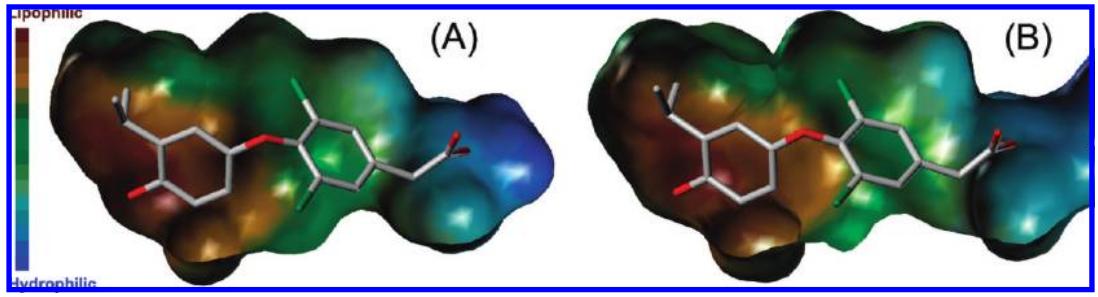

Figure 7. Lipophilicity potential in the binding pocket of the TRs. The Connolly surface of the LBD of the TRs complexed with compound **7** (KB-141) was colored according to the lipophilicity potential generated by the MOLCAD module of SYBYL 8.[12] Only the ligand binding cavity is shown and it is Z-clipped for clarity. (A) TRβ (PDB code 1NAX) and (B) TRα (PDB code 1NAV).

Figure 8. Stereoview of the QSSR CoMFA contour maps, compound **7** (KB-141) is shown as reference. The dots represent the van der Walls radius of the chlorine atom of compound **7**, which is well delimited by three unfavorable steric regions. The small meshes inside the colored contour surfaces were generated by applying a higher contour level, and can be used as a reference (steric contour levels surface −0.1 (yellow) and 0.3 (green), mesh −0.2 and 0.8; electrostatic contour levels surface −0.01 (red) and 0.01 (blue), mesh −0.05 and 0.03).

moderate to high affinity compounds in the data set and present in all TR modulators for which crystallographic structures are available.

The most evident difference is an additional favorable region for bulky groups in the TRβ contour map, represented by the green contour above the 3′ isopropyl group of compound **7** (Figure 6 and Supporting Information Figure 2). Generally, the replacement of the 3′ group by more voluminous substituents leads to a loss of affinity for both isoforms, however in many cases this effect is more evident for TRα, resulting in an increase in TRβ selectivity. These observations suggest that TRβ is more flexible and able to accommodate 3′ bulky groups better than TRα, which is corroborated by the CoMFA affinity contour maps. Interestingly, recent molecular dynamic simulations indicate that one of the escape routes of the ligands from the TR ligand-binding pocket follows the direction of the 3′ substituents.[22,23]

The β isoform also presents an extra contour region near position 1 favoring electronegative substituents (Figure 6 and Supporting Information Figure 2). It should be noticed that, in agreement with previous SAR studies,[12,35] the contour maps indicate that for optimum affinity a propionic acid is favored over an acetic acid substituent (Supporting Information, video 1).

Furthermore, the 3D-QSAR affinity contour maps show that all the steric contours are situated near the distal ring while most of the electrostatic features are close to the carboxylate group on position 1 (see Figure 3 for ring numbering). This aspect reflects the nature of the binding cavities of the TRs in which the environment surrounding the distal ring is highly lipophilic while that near position 1 is populated by polar residues and even water molecules, as observed in the crystallographic structures and depicted in Figure 7. Taken together, these features highlight a number of possible opportunities for the development of analogs with improved affinity.

QSSR Contour Maps. The QSSR CoMFA contour map is depicted in Figure 8. Consistent with the previous discussion, the green contours near the 3′ isopropyl group of compound **7** indicate that larger substituents in this position favor the selectivity toward TRβ, as is the case with the very selective compounds **9**, **11**, **24**, **27**, **34**, and **36**. In

fact, the most selective analog, compound **11**, has its substituent positioned in this region (Supporting Information Figure 3).

The only favorable electrostatic contour region is positioned near the carboxylate group, favoring acetic acid over formic or propionic acids for optimal selectivity, as previously reported.[10] Compounds with negatively charged groups near the blue contour regions will display lower selectivity, while electropositive groups in this position are favored. This tendency is illustrated by the Supporting Information Figure 4, which presents an unselective and a selective compound with these electronic characteristics.

The selectivity for a specific TR isoform results from a combination of the capability of each receptor to accommodate the 3′ group, the 3,5-substituents and the differences in the hydrogen bonding network induced by the substituent at position 1, which usually is a direct consequence of the single amino acid difference between the isoforms. Developing ligands with a 3′ group larger than isopropyl is a common approach for achieving increased selectivity;[11,17,37] however, it is accompanied by a reduction in affinity. Only two crystallographic structures of thyromimetics with a 3′ group larger than isopropyl have been obtained for TRβ and none for TRα,[11,17] making it difficult to fully understand the structural determinants of the selectivity induced by 3′ modifications. On the other hand, substitutions on position 1 yielded compounds with moderate TRβ selectivity while still retaining picomolar affinity.[14,37] The QSSR contour maps indicate that exploring the chemical space around this position may be a promising strategy to obtaining selective ligands which retain high affinity.

An interesting feature of the steric contour map is that the dots representing the van der Waals radius of the chlorine atom of the reference compound are well delimited by three unfavorable steric regions (Figure 8 and Supporting Information Figure 3). This trait is not present in the affinity contour maps, but is in conformity with previous SAR studies,[10,13] indicating that the QSSR model can reliably provide specific information about the selectivity determinants. This characteristic is also observed in a large series of TRβ selective thyromimetics[17,36,39] and the series of highly TRβ selective 6-azauracil-based ligands discovered by Pfizer.[37]

Clearly it is of interest to encounter a plausible structural explanation for the decrease in affinity and increase in selectivity observed when the iodine atoms are replaced by chlorine. Halogen bonds, directional interactions between a halogen atom (chlorine, bromine and iodine) and a nucleophile (usually a carbonyl or hydroxyl group) in which the distance between the two atoms is less than the sum of their van der Waals radii (Figure 9),[40,41] have only recently been recognized as a distinct interaction in ligand recognition and in the assembly of proteins and nucleic acids.[40,42−44] In the case of the TRs, ligands presenting iodine atoms at positions 3 and 5 present higher affinity for both isoforms while compounds with chlorine in these positions display lower affinity and improved TRβ selectivity. The reason may be related to an interaction observed in the X-ray structures of TRα and TRβ in complex with T3 that displays all the features of a halogen bond,[40] but was not previously mentioned in the crystallographic or SAR studies. We noticed that the distance between the atoms involved in the halogen bond is significantly shorter for TRα compared with TRβ (Figure 10) and speculate that this interaction is energetically more favorable in the case of the former, thus reducing the TRβ selectivity of the ligand. The halogen bond is observed in the structures of TRs with cocrystallized ligands containing iodine and bromine, but not chlorine (Figure 9), yet the lack of crystal structures with different ligands for TRα makes it difficult to understand the contribution of this new interaction to the selectivity. It seems possible that the observed unfavorable steric regions identified in the QSSR analysis are an indirect reflection of the existence of the halogen bond itself. Nevertheless, the structure-based pharmacophore derived 3D-QSSR model was able to pinpoint the detrimental contribution of larger halogen atoms to the selectivity, indicating that the methodology presented here is useful in the identification of new structural features related to the activity of the data set compounds.

CONCLUSION

Using a ligand and structure-guided pharmacophore-based methodology, we were able to obtain 3D-QSAR and 3D-QSSR models which exhibited high internal and external consistency. These results show that pharmacophore-based approaches may be of considerable utility in obtaining reliable molecular alignments, particularly in complex cases where rigid body fitting methods and conventional structure-based approaches are unsuccessful. The visual analyses of the affinity and 3D-QSSR contour maps draw attention to a number of new possible opportunities for the development of analogs with improved affinity and selectivity. These may include the exploitation of halogen bonds, which for the first time are described as essential components responsible for the molecular recognition and selectivity of thyroid hormone receptors.

EXPERIMENTAL SECTION

Data Sets. The data set used for the QSAR and QSSR studies contains 69 TR modulators that were selected from the literature.[10−14] Their binding affinity values (as measured by IC_{50}) for both TRα and TRβ were determined by the same research group under standardized experimental conditions as described by Ye,[10] rendering these data comparable between all molecules in the data set, a fundamental requirement for successful QSAR analyses. The IC_{50} values for TRα and TRβ were converted into the corresponding negative logarithmic units, pIC_{50} ($-\log IC_{50}$) and then used in the QSAR studies. The selectivity (S) values for this series of compounds are given by $IC_{50}(TR\alpha)/(IC_{50}(TR\beta) \times 1.7)$,[10] and the logarithm of the selectivity values, defined as log S, was used in the QSSR studies. As the same radiolabeled ligand (T3, compound **1**) was employed in the assays to determine the binding affinities for both TR isoforms, and since this ligand present different affinities for each isoform, the correction factor of 1.7 in the values of selectivity was employed. This correction is derived from the Cheng-Prusoff relationship for competitive inhibitors and was proposed by the authors and subsequently used in studies mentioning the selectivity of these compounds. The chemical structures and corresponding pIC_{50} values for TRα and TRβ, as well as log S, for the complete set of compounds are listed in Table 1.

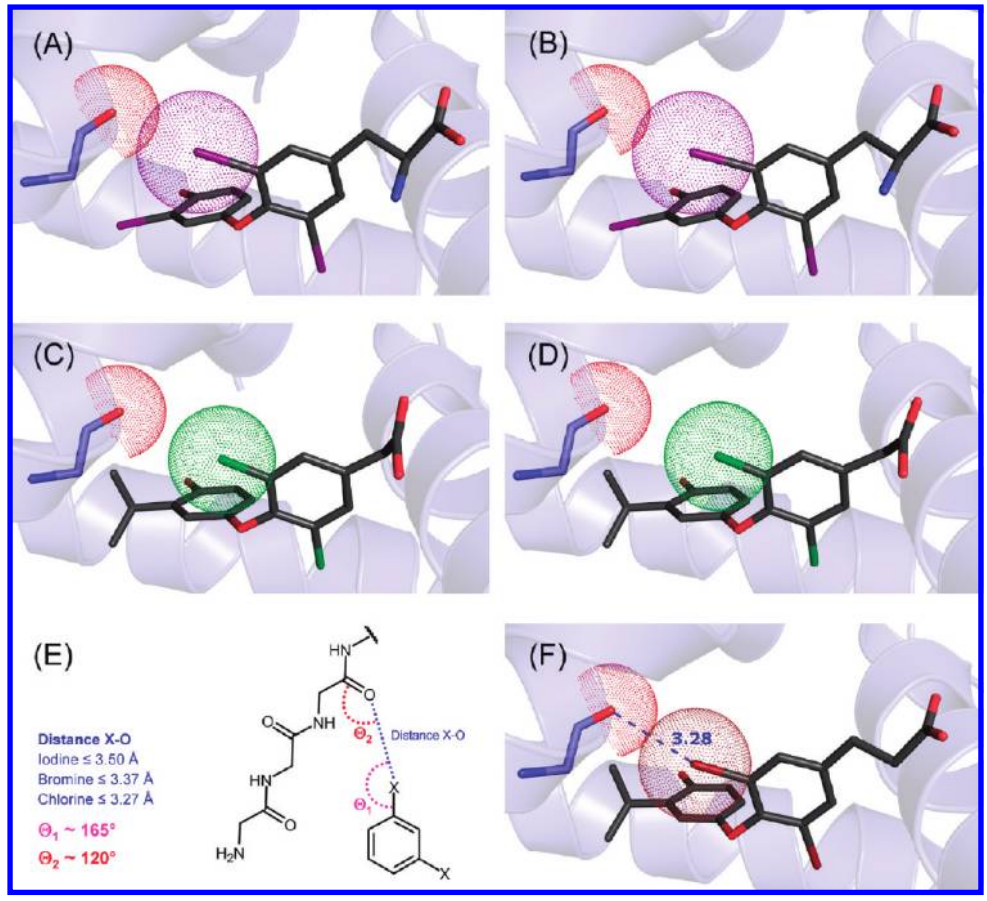

Figure 9. Halogen bond interactions between the TR isoforms and ligands possessing halogen atoms in positions 3 and 5. All the structures were superposed and are shown as a blue transparent cartoon. Only the residue that participates in the halogen bond is shown as sticks, and its side chain has been hidden for clarity. The van der Waals radii of the carbonyl oxygen atom of the protein and the halogen in the ligand are shown as dots. (A) TRα and T3 (PDB code 2H79), (B) TRβ and T3 (PDB code 1XZX), (C) TRα and compound **7** (KB-141) (PDB code 1NAV), (D) TRβ and compound **7** (KB-141) (PDB code 1NAX), and (F) TRβ and compound **4**, which presents bromine atoms in positions 3 and 5 (PDB code 2J4A). (**E**) Simplified scheme of the halogen bond interactions in the thyroid hormone receptors. The reference distances and angles are those described by Auffinger and co-workers.[40] For A, B and F, the distance is shorter than the sum of the van der Waals radii of the oxygen and the halogen atoms, and a halogen bond is observed. In the case of KB-141 (C and D), which has chlorine atoms in positions 3 and 5, the halogen bond is not observed in the crystal structures. See also Figure 10.

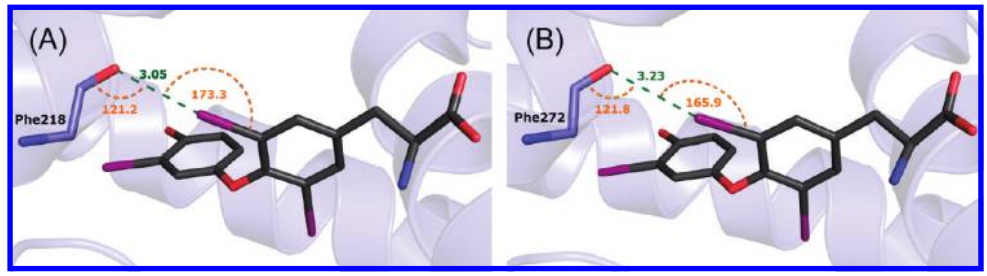

Figure 10. Halogen bond between the TR isoforms and compound **1** (T3). The protein is shown as a transparent blue cartoon. The halogen bonding residue is labeled and shown as sticks, with its side chain hidden for clarity. The T3 iodine atoms are colored in purple. Angles are colored in orange and the distances between the halogen bonding atoms are colored in green. (A) TRα (PDB code 2H79) and (B) TRβ (PDB code 1XZX). For comparison, the sum of the van der Waals radii of oxygen and iodine is 3.50 Å.

Computational Approach. The QSAR and QSSR analyses, calculations, and visualizations for CoMFA were performed using the SYBYL 8 package (Tripos Inc., St. Louis, USA) and Pymol (Delano Software), running on Red Hat Enterprise Linux and Slackware 12.2 Linux workstations, respectively. The 3D structures of the thyromimetics were constructed using the standard geometric parameters of the molecular modeling software package SYBYL 8 and minimized using CONCORD. Before the calculation of the net formal charges, the partial charges and the final geometry used in the CoMFA studies, the carboxylic acids and the basic amines were modeled in their deprotonated and protonated states, respectively. Subsequently each single optimized conformation of each molecule in the data set was energy minimized employing the Tripos force field and Gasteiger—Huckel charges. An alternative approach employing MMFF94 partial charges yielded results which were not statistically different from Gasteiger—Huckel charges and the latter were retained throughout the remainder of the study. Hierarchical cluster analyses of the data set were carried out with Tsar 3D (Accelrys, San Diego, CA).

Pharmacophore Model. Ligand-based pharmacophore models, representing different trade-offs among the conflicting demands of maximizing pharmacophore similarity, increasing steric overlap and minimizing energy strain were generated for different subsets of structurally representative high affinity members of the data set, using the alignment in torsional space of multiple ligands based on shared pharmacophoric and pharmacosteric features as implemented in GALAHAD.[45−47] A representative set of prominent pharmacophore features, taking into account the most promising GALAHAD-derived models, a detailed analysis of the crystallographic structures of the TRs in complex with data set compounds[10,11,19,30] and the previously reported 2D-QSAR studies[29] was used for the construction of the final pharmacophore hypothesis using the program UNITY (Tripos Inc., St. Louis, USA).

Alignment Rule. The CoMFA method requires the specification of both conformations and relative alignments of molecules in the data set, which are the most important adjustable parameters in this method, affecting the outcome of the statistical analysis since the relative interaction energies depend strongly on relative molecular positions.[28,48] The biology of the system, the chemical diversity of the small molecule data set and the availability of reliable structural information about the macromolecular target are the essential aspects that influence the selection of the most appropriate representation of the ligand conformations and the 3D alignment rule. A variety of useful approaches have been described in the literature[31,32,26,48−50] and a pharmacophore-based alignment procedure was used in the present study. The chemical functions of the 3D structures in the data set were geometrically fitted to the positions and relationships between the previously determined 3D features (Figure 3). UNITY was used to generate conformations matching the features in the ligands to those of the pharmacophore model, defining if the candidate structures could reasonably adopt conformations that matched the query. The best fit conformation of each molecule was selected and evaluated, resulting in the data set alignment depicted in Figure 4. The pharmacophore-based molecular alignment of the complete data set was subsequently exploited in the development of predictive CoMFA models. Gasteiger—Huckel charges were assigned to the aligned molecules prior to CoMFA field calculations.

CoMFA Studies. The influence of the steric and electrostatic contributions to the binding affinity and selectivity was studied by using the CoMFA approach. A 3D grid with 2.0 Å spacing was created, sufficient to contain all training set molecules and with an additional 4.0 Å extension in each direction. The steric and electrostatic field energies between the molecules and a sp^3 hybridized carbon atom, with a radius of 1.53 Å and a charge of +1, were respectively calculated according to Lennard-Jones and Coulomb potentials at each lattice intersection of the 3D grid.[28] The region focusing method was employed to increase the resolution of the CoMFA models. The maximum steric and electrostatic energy cutoff was set to 30 kcal mol^{-1}. CoMFA descriptors were used as independent variables, and pIC_{50} values and log *S* values were considered as dependent variables in the partial least-squares (PLS) regression analyses for deducing QSAR and QSSR models, respectively. All CoMFA models were evaluated by the cross-validated (q^2) leave-one-out (LOO) and leave-many-out (LMO) methods, and the sensitivity of the 3D-QSAR models to chance correlation was assessed by the progressive scrambling method. The test set compounds, which were not used in the generation of any of the CoMFA models, were used exclusively in the external validation procedure. In this validation method, the CoMFA models were used to predict the pIC_{50} and log *S* values for the test set compounds, allowing the calculation of the predictive r^2 values (r_{pred}^2) for the QSAR and QSSR models.

ACKNOWLEDGMENT

This work was supported by The State of São Paulo Research Foundation (FAPESP, grants 2008/58316-5 and 1998/14138-2) and The National Council for Scientific and Technological Development (CNPq, grant 150430/2009-4).

Supporting Information Available: Additional figures showing similarities between T3 and KB-141, TRβ affinity contour maps, and QSSR CoMFA steric contour maps and a video file. This material is available free of charge via the Internet at http://pubs.acs.org.

REFERENCES AND NOTES

(1) Ribeiro, R. C.; Kushner, P. J.; Baxter, J. D. The nuclear hormone receptor gene superfamily. *Annu. Rev. Med.* **1995**, *46*, 443–453.
(2) Yen, P. M. Physiological and molecular basis of thyroid hormone action. *Physiol. Rev.* **2001**, *81*, 1097–1142.
(3) Hiroi, Y.; Kim, H. H.; Ying, H.; Furuya, F.; Huang, Z.; Simoncini, T.; Noma, K.; Ueki, K.; Nguyen, N. H.; Scanlan, T. S.; Moskowitz, M. A.; Cheng, S. Y.; Liao, J. K. Rapid nongenomic actions of thyroid hormone. *Proc. Natl. Acad. Sci. U S A* **2006**, *103*, 14104–14109.
(4) Baxter, J. D.; Dillmann, W. H.; West, B. L.; Huber, R.; Furlow, J. D.; Fletterick, R. J.; Webb, P.; Apriletti, J. W.; Scanlan, T. S. Selective modulation of thyroid hormone receptor action. *J. Steroid Biochem. Mol. Biol.* **2001**, *76*, 31–42.
(5) Grover, G. J.; Mellstrom, K.; Ye, L.; Malm, J.; Li, Y. L.; Bladh, L. G.; Sleph, P. G.; Smith, M. A.; George, R.; Vennstrom, B.; Mookhtiar, K.; Horvath, R.; Speelman, J.; Egan, D.; Baxter, J. D. Selective thyroid hormone receptor-beta activation: a strategy for reduction of weight, cholesterol, and lipoprotein (a) with reduced cardiovascular liability. *Proc. Natl. Acad. Sci. U S A* **2003**, *100*, 10067–10072.
(6) Brenta, G.; Danzi, S.; Klein, I. Potential therapeutic applications of thyroid hormone analogs. *Nat. Clin. Pract. Endocrinol. Metab.* **2007**, *3*, 632–640.
(7) Bryzgalova, G.; Effendic, S.; Khan, A.; Rehnmark, S.; Barbounis, P.; Boulet, J.; Dong, G.; Singh, R.; Shapses, S.; Malm, J.; Webb, P.; Baxter, J. D.; Grover, G. J. Anti-obesity, anti-diabetic, and lipid lowering effects of the thyroid receptor beta subtype selective agonist KB-141. *J. Steroid Biochem. Mol. Biol.* **2008**, *111*, 262–267.
(8) Erion, M. D.; Cable, E. E.; Ito, B. R.; Jiang, H.; Fujitaki, J. M.; Finn, P. D.; Zhang, B. H.; Hou, J.; Boyer, S. H.; van Poelje, P. D.; Linemeyer, D. L. Targeting thyroid hormone receptor-beta agonists to the liver reduces cholesterol and triglycerides and improves the therapeutic index. *Proc. Natl. Acad. Sci. U S A* **2007**, *104*, 15490–15495.
(9) Wikstrom, L.; Johansson, C.; Salto, C.; Barlow, C.; Campos Barros, A.; Baas, F.; Forrest, D.; Thoren, P.; Vennstrom, B. Abnormal heart rate and body temperature in mice lacking thyroid hormone receptor alpha 1. *Embo J.* **1998**, *17*, 455–461.
(10) Ye, L.; Li, Y. L.; Mellstrom, K.; Mellin, C.; Bladh, L. G.; Koehler, K.; Garg, N.; Garcia Collazo, A. M.; Litten, C.; Husman, B.; Persson, K.; Ljunggren, J.; Grover, G.; Sleph, P. G.; George, R.; Malm, J. Thyroid receptor ligands. 1. Agonist ligands selective for the thyroid receptor beta1. *J. Med. Chem.* **2003**, *46*, 1580–1588.
(11) Hangeland, J. J.; Doweyko, A. M.; Dejneka, T.; Friends, T. J.; Devasthale, P.; Mellstrom, K.; Sandberg, J.; Grynfarb, M.; Sack, J. S.; Einspahr, H.; Farnegardh, M.; Husman, B.; Ljunggren, J.; Koehler, K.; Sheppard, C.; Malm, J.; Ryono, D. E. Thyroid receptor ligands. Part 2: Thyromimetics with improved selectivity for the thyroid hormone receptor beta. *Bioorg. Med. Chem. Lett.* **2004**, *14*, 3549–3553.
(12) Hedfors, A.; Appelqvist, T.; Carlsson, B.; Bladh, L. G.; Litten, C.; Agback, P.; Grynfarb, M.; Koehler, K. F.; Malm, J. Thyroid receptor ligands. 3. Design and synthesis of 3,5-dihalo-4-alkoxyphenylalkanoic

acids as indirect antagonists of the thyroid hormone receptor. *J. Med. Chem.* **2005**, *48*, 3114–3117.
(13) Li, Y. L.; Litten, C.; Koehler, K. F.; Mellstrom, K.; Garg, N.; Garcia Collazo, A. M.; Farnegard, M.; Grynfarb, M.; Husman, B.; Sandberg, J.; Malm, J. Thyroid receptor ligands. Part 4: 4′-amido bioisosteric ligands selective for the thyroid hormone receptor beta. *Bioorg. Med. Chem. Lett.* **2006**, *16*, 884–886.
(14) Garcia Collazo, A. M.; Koehler, K. F.; Garg, N.; Farnegardh, M.; Husman, B.; Ye, L.; Ljunggren, J.; Mellstrom, K.; Sandberg, J.; Grynfarb, M.; Ahola, H.; Malm, J. Thyroid receptor ligands. Part 5: novel bicyclic agonist ligands selective for the thyroid hormone receptor beta. *Bioorg. Med. Chem. Lett.* **2006**, *16*, 1240–1244.
(15) Baxter, J. D.; Webb, P.; Grover, G.; Scanlan, T. S. Selective activation of thyroid hormone signaling pathways by GC-1: a new approach to controlling cholesterol and body weight. *Trends Endocrinol. Metab.* **2004**, *15*, 154–157.
(16) Scanlan, T. S. Sobetirome: a case history of bench-to-clinic drug discovery and development. *Heart Fail. Rev.* **2008**, DOI: 10.1007/s10741-008-9122-x.
(17) Borngraeber, S.; Budny, M. J.; Chiellini, G.; Cunha-Lima, S. T.; Togashi, M.; Webb, P.; Baxter, J. D.; Scanlan, T. S.; Fletterick, R. J. Ligand selectivity by seeking hydrophobicity in thyroid hormone receptor. *Proc. Natl. Acad. Sci. U S A* **2003**, *100*, 15358–15363.
(18) Togashi, M.; Borngraeber, S.; Sandler, B.; Fletterick, R. J.; Webb, P.; Baxter, J. D. Conformational adaptation of nuclear receptor ligand binding domains to agonists: potential for novel approaches to ligand design. *J. Steroid Biochem. Mol. Biol.* **2005**, *93*, 127–137.
(19) Darimont, B. D.; Wagner, R. L.; Apriletti, J. W.; Stallcup, M. R.; Kushner, P. J.; Baxter, J. D.; Fletterick, R. J.; Yamamoto, K. R. Structure and specificity of nuclear receptor-coactivator interactions. *Genes Dev.* **1998**, *12*, 3343–3356.
(20) Valadares, N. F.; Polikarpov, I.; Garratt, R. C. Ligand induced interaction of thyroid hormone receptor beta with its coregulators. *J. Steroid Biochem. Mol. Biol.* **2008**, *112*, 205–212.
(21) Webb, P.; Nguyen, N. H.; Chiellini, G.; Yoshihara, H. A.; Cunha Lima, S. T.; Apriletti, J. W.; Ribeiro, R. C.; Marimuthu, A.; West, B. L.; Goede, P.; Mellstrom, K.; Nilsson, S.; Kushner, P. J.; Fletterick, R. J.; Scanlan, T. S.; Baxter, J. D. Design of thyroid hormone receptor antagonists from first principles. *J. Steroid Biochem. Mol. Biol.* **2002**, *83*, 59–73.
(22) Martínez, L.; Webb, P.; Polikarpov, I.; Skaf, M. S. Molecular dynamics simulations of ligand dissociation from thyroid hormone receptors: evidence of the likeliest escape pathway and its implications for the design of novel ligands. *J. Med. Chem.* **2006**, *49*, 23–26.
(23) Martinez, L.; Polikarpov, I.; Skaf, M. S. Only subtle protein conformational adaptations are required for ligand binding to thyroid hormone receptors: Simulations using a novel multi-point steered molecular dynamics approach. *J. Phys. Chem. B* **2008**, *112*, 10741–10751.
(24) Cherkasov, A.; Ban, F.; Santos-Filho, O.; Thorsteinson, N.; Fallahi, M.; Hammond, G. L. An updated steroid benchmark set and its application in the discovery of novel nanomolar ligands of sex hormone-binding globulin. *J. Med. Chem.* **2008**, *51*, 2047–2056.
(25) Chen, C. K.-M.; Hudock, M. P.; Zhang, Y.; Guo, R. T.; Cao, R.; No, J. H.; Liang, P. H.; Ko, T. P.; Chang, T. H.; Chang, S. C.; Song, Y.; Axelson, J.; Kumar, A.; Wang, A. H.; Oldfield, E. Inhibition of geranylgeranyl diphosphate synthase by bisphosphonates: a crystallographic and computational investigation. *J. Med. Chem.* **2008**, *51*, 5594–5607.
(26) Salum, L. B.; Polikarpov, I.; Andricopulo, A. D. Structure-based approach for the study of estrogen receptor binding affinity and subtype selectivity. *J. Chem. Inf. Model.* **2008**, *48*, 2243–2253.
(27) Cramer, R. D., 3rd; Patterson, D. E.; Bunce, J. D. Recent advances in comparative molecular field analysis (CoMFA). *Prog. Clin. Biol. Res.* **1989**, *291*, 161–165.
(28) Cramer, R. D.; Patterson, D. E.; Bunce, J. D. Comparative Molecular-Field Analysis (Comfa) 0.1. Effect of Shape on Binding of Steroids to Carrier Proteins. *J. Am. Chem. Soc.* **1988**, *110*, 5959–5967.
(29) Valadares, N. F.; Castilho, M. S.; Polikarpov, I.; Garratt, R. C. 2D QSAR studies on thyroid hormone receptor ligands. *Bioorg. Med. Chem.* **2007**, *15*, 4609–4617.
(30) Sandler, B.; Webb, P.; Apriletti, J. W.; Huber, B. R.; Togashi, M.; Cunha Lima, S. T.; Juric, S.; Nilsson, S.; Wagner, R.; Fletterick, R. J.; Baxter, J. D. Thyroxine-thyroid hormone receptor interactions. *J. Biol. Chem.* **2004**, *279*, 55801–55808.
(31) Castilho, M. S.; Postigo, M. P.; de Paula, C. B.; Montanari, C. A.; Oliva, G.; Andricopulo, A. D. Two- and three-dimensional quantitative structure-activity relationships for a series of purine nucleoside phosphorylase inhibitors. *Bioorg. Med. Chem.* **2006**, *14*, 516–527.
(32) Guido, R. V.; Oliva, G.; Montanari, C. A.; Andricopulo, A. D. Structural basis for selective inhibition of trypanosomatid glyceraldehyde-3-phosphate dehydrogenase: molecular docking and 3D QSAR studies. *J. Chem. Inf. Model.* **2008**, *48*, 918–929.
(33) Chen, Y.; Li, H.; Tang, W.; Zhu, C.; Jiang, Y.; Zou, J.; Yu, Q.; You, Q. 3D-QSAR studies of HDACs inhibitors using pharmacophore-based alignment. *Eur. J. Med. Chem.* **2008**, *44*, 2868–2876.
(34) Nascimento, A. S.; Dias, S. M.; Nunes, F. M.; Aparicio, R.; Ambrosio, A. L.; Bleicher, L.; Figueira, A. C.; Santos, M. A.; de Oliveira Neto, M.; Fischer, H.; Togashi, M.; Craievich, A. F.; Garratt, R. C.; Baxter, J. D.; Webb, P.; Polikarpov, I. Structural rearrangements in the thyroid hormone receptor hinge domain and their putative role in the receptor function. *J. Mol. Biol.* **2006**, *360*, 586–598.
(35) Koehler, K.; Gordon, S.; Brandt, P.; Carlsson, B.; Backsbro-Saeidi, A.; Apelqvist, T.; Agback, P.; Grover, G. J.; Nelson, W.; Grynfarb, M.; Farnegardh, M.; Rehnmark, S.; Malm, J. Thyroid receptor ligands. 6. A high affinity "direct antagonist" selective for the thyroid hormone receptor. *J. Med. Chem.* **2006**, *49*, 6635–6637.
(36) Wagner, R. L.; Huber, B. R.; Shiau, A. K.; Kelly, A.; Cunha Lima, S. T.; Scanlan, T. S.; Apriletti, J. W.; Baxter, J. D.; West, B. L.; Fletterick, R. J. Hormone selectivity in thyroid hormone receptors. *Mol. Endocrinol.* **2001**, *15*, 398–410.
(37) Dow, R. L.; Schneider, S. R.; Paight, E. S.; Hank, R. F.; Chiang, P.; Cornelius, P.; Lee, E.; Newsome, W. P.; Swick, A. G.; Spitzer, J.; Hargrove, D. M.; Patterson, T. A.; Pandit, J.; Chrunyk, B. A.; LeMotte, P. K.; Danley, D. E.; Rosner, M. H.; Ammirati, M. J.; Simons, S. P.; Schulte, G. K.; Tate, B. F.; DaSilva-Jardine, P. Discovery of a novel series of 6-azauracil-based thyroid hormone receptor ligands: potent, TR beta subtype-selective thyromimetics. *Bioorg. Med. Chem. Lett.* **2003**, *13*, 379–382.
(38) Du, J.; Qin, J.; Liu, H.; Yao, X. 3D-QSAR and molecular docking studies of selective agonists for the thyroid hormone receptor beta. *J. Mol. Graph. Model.* **2008**, *27*, 95–104.
(39) Chiellini, G.; Nguyen, N. H.; Apriletti, J. W.; Baxter, J. D.; Scanlan, T. S. Synthesis and biological activity of novel thyroid hormone analogues: 5′-aryl substituted GC-1 derivatives. *Bioorg. Med. Chem.* **2002**, *10*, 333–346.
(40) Auffinger, P.; Hays, F. A.; Westhof, E.; Ho, P. S. Halogen bonds in biological molecules. *Proc Natl Acad Sci U S A* **2004**, *101*, 16789–16794.
(41) Politzer, P.; Lane, P.; Concha, M. C.; Ma, Y.; Murray, J. S. An overview of halogen bonding. *J. Mol. Model.* **2007**, *13*, 305–311.
(42) Voth, A. R.; Hays, F. A.; Ho, P. S. Directing macromolecular conformation through halogen bonds. *Proc Natl Acad Sci U S A* **2007**, *104*, 6188–6193.
(43) Metrangolo, P.; Resnati, G. Halogen versus hydrogen. *Science* **2008**, *321*, 918–919.
(44) Lu, Y.; Shi, T.; Wang, Y.; Yang, H.; Yan, X.; Luo, X.; Jiang, H.; Zhu, W. Halogen bonding—A novel interaction for rational drug design. *J. Med. Chem.* **2009**, *52*, 2854–2862.
(45) Richmond, N. J.; Abrams, C. A.; Wolohan, P. R.; Abrahamian, E.; Willett, P.; Clark, R. D. GALAHAD: 1. pharmacophore identification by hypermolecular alignment of ligands in 3D. *J. Comput.-Aided Mol. Des* **2006**, *20*, 567–587.
(46) Shepphird, J. K.; Clark, R. D. A marriage made in torsional space: Using GALAHAD models to drive pharmacophore multiplet searches. *J. Comput.-Aided Mol. Des.* **2006**, *20*, 763–771.
(47) Clark, R. D.; Abrahamian, E. Using a staged multi-objective optimization approach to find selective pharmacophore models. *J. Comput. Aided Mol. Des.* **2008**, DOI: 10.1007/s10822-008-9227-2.
(48) Sutherland, J. J.; O'Brien, L. A.; Weaver, D. F. A comparison of methods for modeling quantitative structure-activity relationships. *J. Med. Chem.* **2004**, *47*, 5541–5554.
(49) Tintori, C.; Corradi, V.; Magnani, M.; Manetti, F.; Botta, M. Targets looking for drugs: a multistep computational protocol for the development of structure-based pharmacophores and their applications for hit discovery. *J. Chem. Inf. Model.* **2008**, *48*, 2166–2179.
(50) Salum, L. B.; Polikarpov, I.; Andricopulo, A. D. Structural and chemical basis for enhanced affinity and potency for a large series of estrogen receptor ligands: 2D and 3D QSAR studies. *J. Mol. Graph. Model.* **2007**, *26*, 434–442.

CI900316E